

Tuning the thermal conductivity of silicon nanowires by surface passivation

Céline Ruscher,¹ Robinson Cortes-Huerto,² Robert Hannebauer,³
Debashish Mukherji,^{4,*} Alireza Nojeh,^{5,4} and A. Srikantha Phani¹

¹*Department of Mechanical Engineering, University of British Columbia, Vancouver BC V6T 1Z4, Canada*

²*Max-Planck Institut für Polymerforschung, Ackermannweg 10, 55128 Mainz, Germany*

³*Lumiense Photonics Inc., Vancouver, Canada*

⁴*Quantum Matter Institute, University of British Columbia, Vancouver BC V6T 1Z4, Canada*

⁵*Department of Electrical and Computer Engineering,
University of British Columbia, Vancouver BC V6T 1Z4, Canada*

Using large scale molecular dynamics simulations, we study the thermal conductivity of bare and surface passivated silicon nanowires (SiNWs). For the cross-sectional widths $w \leq 2$ nm, SiNWs become unstable because of the surface amorphousization and also due to the evaporation of a certain fraction of Si atoms. The observed surface (in-)stability is related to a large excess energy Δ of the surface Si atoms with respect to the bulk Si, resulting from the surface atoms being less coordinated and having dangling bonds. We first propose a practically relevant method that uses Δ as a guiding tool to passivate these dangling bonds with hydrogen or oxygen, stabilizing the SiNWs. These passivated SiNWs are used to calculate the thermal conductivity coefficient κ . While the expected trend of $\kappa \propto w$ is observed for all SiNWs, surface passivation provides an added flexibility of tuning κ with the surface coverage concentration c of passivated atoms. Indeed, with respect to the bulk κ , passivation of SiNW reduces κ by 75–80% for $c \rightarrow 50\%$ and recovers again by 50% for the fully passivated samples. Analyzing the phonon band structures via spectral energy density, we discuss separate contributions from the surface and the core to κ . Our results also reveal that surface passivation increases SiNW stiffness, contributing to the tunability in κ .

I. INTRODUCTION

Silicon (Si) is an important building block in designing nanoscale devices [1–6], where tuning its physical properties, such as thermal and/or electrical transport, and mechanical stability, is an essential for their use in a desired application. In this context, the ability to conduct the heat current is one of the key properties that dictates the applicability of a material under a wide range of environmental conditions [7]. For example, a high thermal transport coefficient κ is needed for a heat sink material, while a low κ is required for an high efficiency thermoelectric device [8–11].

To achieve a desired (predictive) level of tunability in κ , silicon nanowire (SiNW) sensors are of particular interest [5, 6, 8]. In particular, decrease in κ was observed by changing the morphology via introducing kinks or pores [12–14], roughness [15], and the cross-sectional shapes [16]. Tuning the mechanical property of SiNWs has also shown promising results, which may be achieved by introducing point defects in the crystalline lattice, and thus κ was shown to reduce by about 70% [17].

In the ongoing quest toward structural miniaturization, there is also a need to better understand these materials at the nanoscale, especially when the cross-section width $w \leq 10$ nm. For nano-materials, lateral miniaturization often leads to a significant variation in κ [8, 15, 18–22]. In particular, under strong confinement a delicate balance between the bulk as well as the surface phonon propaga-

tion controls κ [23–25]. For example, it has been experimentally shown that κ of SiNWs can be reduced by over an order of magnitude with respect to the bulk Si when $w \approx 22$ nm [18]. However, a significant challenge here is to attain a stable SiNW structure in the simulations for the smaller w values [25, 26]. When w is small, i.e., only about a few tens of unit cells, surfaces of a free-standing SiNW become amorphous [27], while the core remains fairly crystalline. In some cases, even the surface Si atoms evaporate. This behavior is a result of the dangling bonds on the surfaces that originate because of the less coordinated surface Si atoms, and is not only known for SiNWs in the context of the electronic-band-structure [28], but is also observed for the stability of metal nanoparticles [29, 30].

A common practical treatment to eliminate surface disorder is by the passivation of the surface dangling bonds [31–34]. In this context, while there are several experimental studies highlighting the importance of surface passivation, to the best of our knowledge, simulation studies on the exact role of surface passivation on SiNW stability and its connection to κ are rather limited. Computational studies, however, dealt with surface-nitrogenation [35] and engineered surface-amorphousization [24]. In both cases, a layer of hydrogen atoms was introduced on the surfaces, without explicitly discussing the effects of hydrogen. Furthermore, we also note in passing that using N on Si is a rather nontrivial practical task because they usually induce large differential stresses and may make a surface unstable. Therefore, a detailed structure-property relationship is needed that may be used for the rational understanding and functional design of engineered advanced materials with sta-

*debashish.mukherji@ubc.ca

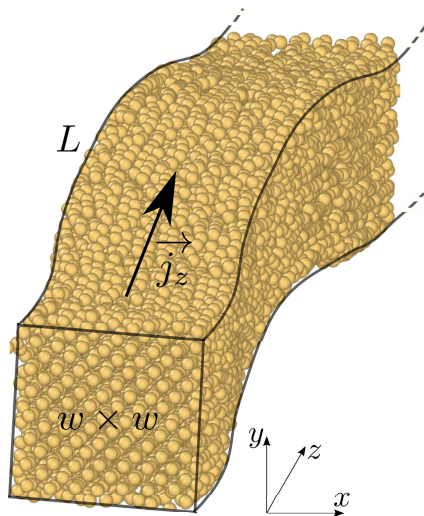


FIG. 1: A simulation snapshot of an equilibrated bare silicon nano-wire (SiNW) with a cross-section width $w = 4.34$ nm and a length $L = 69.52$ nm. The thermal transport coefficient κ is calculated along the z -direction and \vec{j}_z is the heat flux, which is the $\langle 100 \rangle$ crystalline plane oriented.

ble surfaces.

Motivated by the above discussion, we study the κ behavior in SiNWs with the goals to: (1) establish a structure-property relationship in SiNWs, (2) study the surface stability by using the excess energy Δ as a guiding tool and the effect of passivation on Δ , (3) show how the surface passivation can lead to additional flexibility in tuning κ , and (4) discuss separate contributions of the surface and the core to the κ behavior as revealed by the phonon band structures. To achieve these goals, we employ a large scale atomistic molecular dynamics simulation protocol.

The remainder of the paper is organized as follows: in Section II we sketch a detailed discussion of the simulation model and method. Results are presented in Section III and finally conclusions are drawn in Section IV.

II. MODEL AND METHODS

Individual systems consist of free-standing SiNW of length $L = 128a$ and the cross-section is chosen as a square geometry with the varying width w that is taken between $4a$ and $24a$. Here, $a \simeq 0.54$ nm is the lattice constant. This leads to the typical number of particles N per system varying between $1.63 \times 10^4 - 5.89 \times 10^5$. We consider the $\langle 100 \rangle$ crystalline plane oriented along the z -axis, i.e., the direction of κ calculation. A representative simulation snapshot of a bare SiNW highlighting the direction of heat flow is shown in Fig. 1. The bare-SiNWs are also passivated with oxygen (O-SiNW) or hydrogen (H-SiNW).

The initial configurations are created by placing a SiNW at the center of a simulation box with dimensions $50w \times$

$50w \times L$. The periodic boundary conditions are applied along all directions, but a large vacuum in the lateral directions (i.e., along x - and y -directions) prevents the Si atoms from seeing their periodic images due to the flexural vibrations and thus precludes any simulation artifacts.

The Tersoff potential is used for the silicon (Si) interactions [36]. A set of modified Tersoff parameters are used to mimic the interactions of Si with oxygen (O-SiNW) [37] and hydrogen (H-SiNW) [38].

The temperature T is imposed using the Nosé-Hoover thermostat. Unless stated otherwise all physical properties are calculated at $T = 600$ K. At different stages of simulations, spurious structural stresses along the z -direction are relaxed under NpT simulation, where pressure $p = 1$ atm is also imposed using the Nosé-Hoover barostat. The equations of motion are integrated using the Verlet algorithm. The integration time step Δt for SiNWs and O-SiNWs is 1.0 fs, while $\Delta t = 0.1$ fs is chosen for H-SiNWs. The GPU-accelerated LAMMPS package is used for these simulations [39].

A. Equilibration of the free-standing SiNWs

To achieve a stable free standing SiNW structure, the initial structural equilibration is performed in different steps:

1. The crystalline SiNW structures are initially created at $T = 0$ K.
2. Subsequently a SiNW is heated to $T = 10$ K for a time $t = 10^2$ ps.
3. The final configurations from step 2 are then heated further to $T = 600$ K for $t = 10^3$ ps. For some test simulations, configurations are also created at $T = 300$ K.
4. The configurations from the step 3 are then further equilibrated at $T = 600$ K for $t = 10^3$ ps.

We note in passing that in steps 2-4, simulations are performed under an anisotropic pressure coupling that is only employed along the z -direction, i.e., along the SiNW length. The final configurations obtained after step 4 are equilibrated in the canonical ensemble for an additional $t = 4 \times 10^3$ ps. We would also like to emphasize that a rather complex sample preparation protocol is used to ensure that the well-defined (residual stress-free) SiNW structures are obtained.

B. Passivation of the free surface

The surface passivated systems (O-SiNW and H-SiNW) are prepared at different surface coverage concentrations c . Here, $c = 1.0$ is defined as the maximum number of

passivating atoms that can be added without introducing more dangling bonds by the passivation. In the case of O–SiNW, one oxygen can bind to two Si atoms and thus leaves a small fraction of dangling bonds even for $c = 1.0$. In H–SiNW, however, all dangling bonds are passivated because of their single Si–H coordination. Subsequently, the samples with different c are generated by randomly removing $(1 - c)$ fraction of passivating atoms.

C. Thermal transport coefficient calculations

The thermal transport coefficient κ is calculated using the approach-to-equilibrium (ATE) method [40]. Within this method, L along the direction of heat flow is subdivided into three layers, i.e., $0 - L/4$ (layer I), $L/4 - 3L/4$ (layer II) and $3L/4 - L$ (layer III). In the first stage of canonical simulation, layers I and III are thermalized at $T_h = T + 100$ K, while the layer II is kept at $T_c = T - 100$ K. After this thermalization stage, simulations are performed in the microcanonical ensemble that allows for the redistribution of energy, where $\Delta T = T_h - T_c$ are allowed to relax. As proposed in Ref. [40], we fit ΔT by a bi-exponential function $\Delta T = c_1 \exp(-t/\tau_1) + c_{\parallel} \exp(-t/\tau_{\parallel})$ and obtain the time constant τ_{\parallel} along the direction of heat flow. Finally κ can be calculated using,

$$\kappa = \frac{1}{4\pi^2} \frac{Lc_v}{w^2\tau_{\parallel}}, \quad (1)$$

where c_v is the heat capacity. We have used the Dulong–Petit classical estimate for $c_v = 3Nk_B$, with k_B being the Boltzmann constant and N is the total number of atoms in a system.

The calculations are performed at $T = 600$ K because the temperature equilibration in NVT and the subsequent relaxation in NVE for κ calculations can be achieved within a reasonable simulation time without any unphysical energy drift. Note that the microcanonical simulations (especially with complex empirical potentials) typically show an energy drift over long times and for relatively large Δt [41]. Furthermore, even when we are performing simulations at $T = 600$ K, the bare crystalline structure remains stable because $600 \text{ K} < \Theta_D$ [42]. Here, Θ_D is the Debye temperature and for this model $\Theta_D \geq 640$ K [43]. The results of κ for SiNW, O–SiNW, and H–SiNW are presented in comparison to the bulk thermal transport coefficient κ_{bulk} . In our simulations, κ_{bulk} is calculated in a $10a \times 10a \times 128a$ Si sample with PBC in all directions, i.e., without a large vacuum in the lateral directions. This calculated $\kappa_{\text{bulk}}^{\text{Si}} \simeq 10.1 \pm 1.3$ W/Km is consistent with an earlier simulation data in Ref. [40] for $L \simeq 69.52$ nm, while is about a factor of six smaller than the known experimental value $\kappa_{\text{bulk}}^{\text{exp}} \simeq 65$ W/Km [44]. The observed variation between our simulation results and the experimental values is because κ is L -dependent [40, 45] when calculated using a non-equilibrium method, as in the ATE method. This is particularly due to the reason that the phonon wavelength is truncated along the

direction of heat flow due to the boundary scattering. Furthermore, the central goal of our work is to investigate the change in κ by passivation. Therefore, we do not go into more detail on the length effects on κ and its value in the asymptotic limit. The latter can however be estimated to be $\kappa \simeq 145$ W/Km by extrapolating the data in Ref. [40] for the same method and same model as ours. We have also attempted to calculate $\kappa_{\text{bulk}}^{\text{Si}}$ using the equilibrium Kubo–Green method [46], where the system size effects may be reduced. We, however, had severe problems with the convergence of heat flux auto-correlation function and drift in energy under NVE (data not shown).

D. Spectral energy density calculation

The phonon band structure is calculated using the spectral energy density (SED) $\phi(k, \nu)$ [47–49]. In our study, we define a supercell of Si atoms within a region of size $4a \times 4a \times a$ that in total has $N_{\text{supercell}} = N_x N_y N_z = 128$ atoms per supercell. Here, $\phi(k, \nu)$ is estimated using,

$$\phi(k, \nu) = \frac{1}{4\pi\tau_0 N_T} \sum_{\alpha} \sum_b^B m_b \left| \int_0^{\tau_0} \sum_l^{N_T} \dot{u}_{\alpha}^{l,b}(t) \exp(ik \cdot r_0^l - i\nu t) dt \right|^2, \quad (2)$$

where $\dot{u}_{\alpha}^{l,b}$ is the velocity of the $\alpha = \{x, y, z\}$ coordinate of the b particle of mass m_b in the unit supercell l . r_0^l corresponds to the equilibrium position of the l supercell. We note in passing that Eq. 2 is based on a normal mode analysis in the frequency domain that does not rely on the phonon eigenvectors, instead only on the Fourier transform of the atoms velocities [50] obtained over a total time τ_0 . Using the equilibrated configurations, we run NVE simulations for 2ns per sample with $\Delta t = 0.5$ fs for SiNWs and O–SiNWs and $\Delta t = 0.05$ fs for H–SiNWs. Velocities and positions are stored every 16 fs.

III. RESULTS AND DISCUSSIONS

A. Surface stability and excess energy

We begin by discussing the surface stability of SiNWs. For this purpose, we show a simulation snapshot of bare SiNW in Fig. 1. It can be appreciated that—even when the core of SiNW is crystalline, there is visibly a large degree of rearrangement of the surface Si atoms, forming an amorphous surface layer. To quantify this surface disorder and its correlation with the surface energy, we have calculated the excess energy using [51, 52]

$$\Delta = \frac{E(N) - N\varepsilon_B^{\text{Si}}}{N^{2/3}}, \quad (3)$$

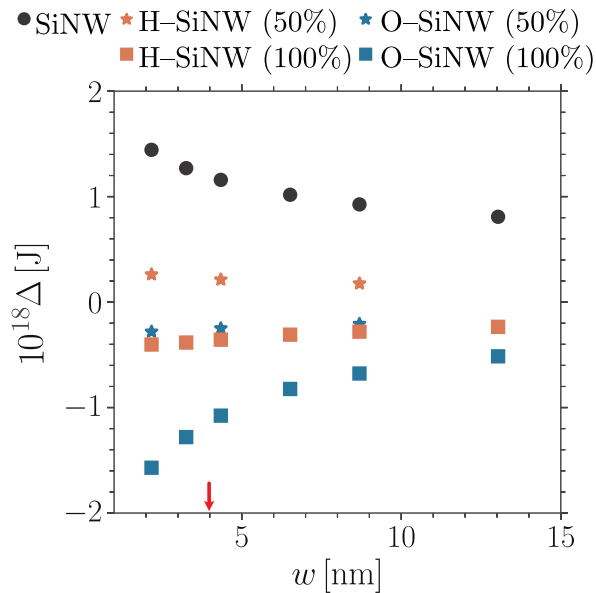


FIG. 2: The excess energy Δ of the surface Si atoms as a function of the cross-section width w of the silicon nanowires (SiNWs). The data is shown for a temperature $T = 600$ K and for two different surface coverage concentrations c , i.e., 50% and 100%. Red arrow indicates at a w value that corresponds to the simulation snapshot in Figs. 1 and 3.

where Δ is calculated relative to the bulk cohesion energy per atom $\varepsilon_B^{\text{Si}}$ of bare Si and the energy of a SiNW with N atoms is given by $E(N)$. The factor $N^{2/3}$ scales as the number of surface atoms. The variation of Δ with w is shown in Fig. 2.

A closer look at the bare SiNW data (see the black \bullet data set) shows that Δ increases monotonically with decreasing w and thus indicates that the surface effects become more dominant for smaller w . This Δ variation with w is also directly related to the stability of SiNWs, especially for smaller w where creating a surface usually has a significant energy cost. Furthermore, we note that even when Δ decreases with w , it still remains significantly large for $w \rightarrow 13.0$ nm (i.e., $\Delta \simeq 10^{-18}$ J or $\simeq 120 k_B T$ at $T = 600$ K) and thus the surfaces remain fairly disordered for all w , see also the Supplementary Fig. S1(a) [53].

The central cause of such disorder is that the Si atoms are less coordinated on the surfaces than in the bulk and thus have a substantial number of dangling bonds. This contributes to a large energy penalty in forming a surface. Indeed, the surface energy, to a first approximation, is proportional to the total number of broken bonds at the surface [29]. Furthermore, it has also been shown that the Si-Si bond length decreases on the surface in comparison to the core [54]. Such lattice contraction has been reported both in simulations and in experiments for Si nano-clusters [55, 56]. Likewise, our simulations also reproduce this behavior of lattice contraction. More specifically, cross-sectional surface area of a bare SiNW with $w = 4a$ is $\mathcal{A}_{\text{cross}} \simeq 4.05 \text{ nm}^2$, which is about 14%

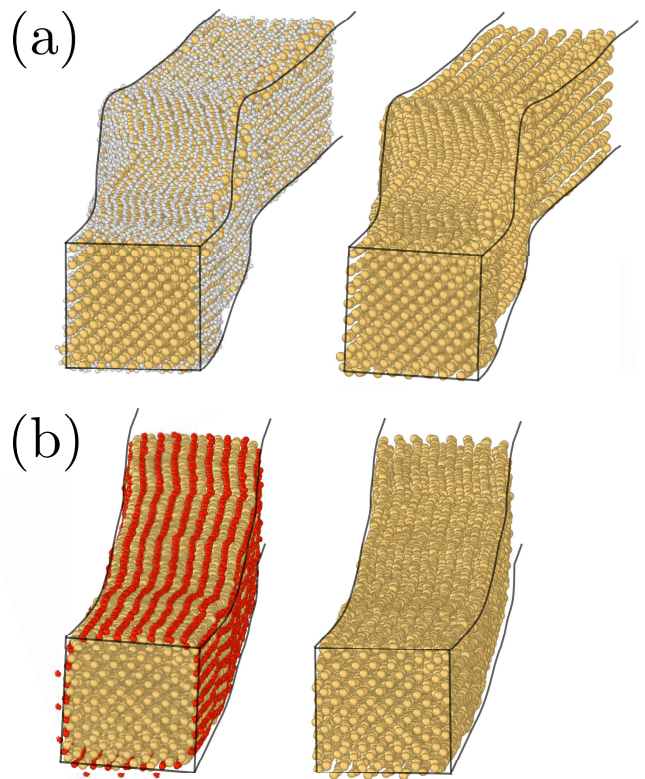


FIG. 3: Simulation snapshots showing the passivated silicon nano-wire (SiNW) by hydrogen (part a) and oxygen (part b) for a cross-section width $w = 4.34$ nm. Snapshots are rendered with (left panels) and without (right panels) the passivated atoms. These simulation snapshots are shown for 100% surface coverage concentration c of the passivated atoms. To obtain configurations at different c , corresponding numbers of passivated atoms are randomly removed from the surface.

smaller than the expected value of 4.72 nm^2 for a perfect lattice. This has a direct implication on the elastic bending and torsional stiffness of the passivated SiNWs as we shall see later.

There are different treatments to eliminate surface disorder. Here, a common industrially relevant procedure is to deposit 5–10 nm of either silicon dioxide (SiO_2) or silicon nitride (SiNH_3) on bare SiNWs [31–34]. This serves as a natural route to reduce Δ as it reduces the number of dangling bonds. Simulations have also shown that passivation using amorphous Si [24] or hydrogen [54, 57] may stabilize the surfaces. We take motivation from these experimental and simulation studies and passivate SiNW surfaces with either oxygen (O-SiNW) or hydrogen (H-SiNW). The latter is specifically chosen because hydrogen-on-silicon is used for inorganic solar cells[58] and/or for data storage [59]. Note that we passivate the SiNW surfaces with only a monolayer of atoms.

In Fig. 3 we show 100% passivated SiNWs, with (left panel) and without (right panel) rendering the passivated atoms. As expected, passivation helps preserving the

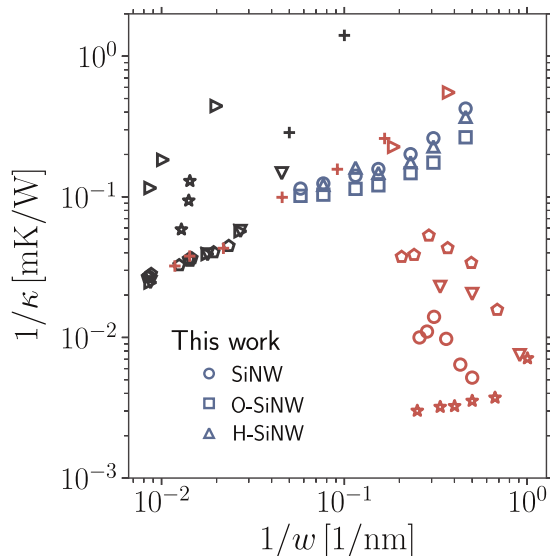


FIG. 4: Inverse thermal transport coefficient $1/\kappa$ as a function inverse of cross-section width $1/w$ for different nanowires. The data from this work is shown for the bare silicon nanowires (SiNW), SiNW passivated with oxygen (O-SiNW), and SiNW passivated with hydrogen (H-SiNW), see the blue data sets. Results are only shown for the 100% surface passivation coverage. κ is calculated at a temperature of $T = 600$ K. For the comparison, we have also included data from the earlier published simulations (red data sets) [20, 22, 23, 25, 61, 62] and experiments (black data sets) [8, 15, 18, 19, 63]. We note in passing that we have also calculated the error bars from a set of six independent simulation runs for each configuration. However, the error bars are not properly visible in a log-log plot with several decades on both the axes. Therefore, the raw κ vs w data (including their error bars) for all the samples are shown in the Supplementary Fig. S4.

crystallinity of the O-SiNW and H-SiNW surfaces (see the right panels in Fig. 3) in comparison to bare SiNW in Fig. 1.

Passivation also significantly reduces Δ , see the \star and \blacksquare data sets in Fig. 2. It can be seen that Δ remains almost constant for all passivated systems, except for O-SiNW with 100% passivation, see blue \blacksquare data set in Fig. 2. This observed large negative Δ for O-SiNW can be understood by assessing the different contributions in Eq. 3. For example, Δ in Eq. 3 is estimated relative to $\varepsilon_B^{\text{Si}}$, which only includes Si-Si binding energy. Here, the Si-Si binding energy is about 222 kJ/mol, while the Si-O binding energy can be as high as 452 kJ/mol [60]. These two separate contributions together will then result in a difference greater than just bare $\varepsilon_B^{\text{Si}}$ in Eq. 3. This correction is then expected to lead to a smaller negative magnitude of Δ for O-SiNW. Note that these binding energy estimates are obtained at $T = 273$ K and our simulations are performed at $T = 600$ K. Therefore, it may not be trivial to straightforwardly apply these estimates to our calculations.

For H-SiNW, the reported H-H and Si-H binding ener-

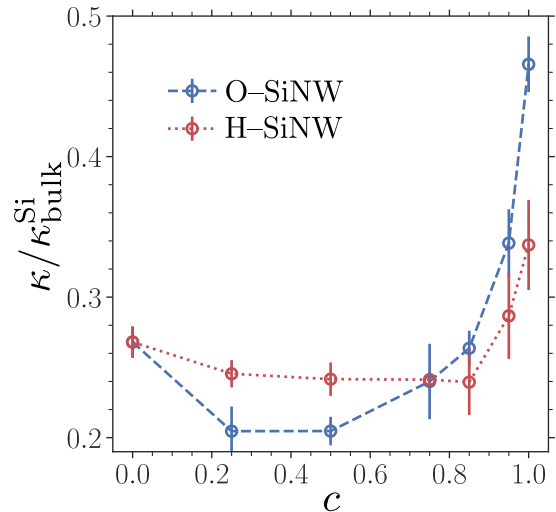


FIG. 5: Normalized thermal transport coefficient $\kappa/\kappa_{\text{bulk}}^{\text{Si}}$ as a function of surface coverage concentration of the passivated atoms c . Here $\kappa_{\text{bulk}}^{\text{Si}} = 10.1 \pm 1.3$ W/mK. Data is shown for a temperature of $T = 600$ K and for two different passivations, i.e., oxygen (O-SiNW) and hydrogen (H-SiNW). Individual κ values are the averages of six independent runs and the error bars are standard deviation.

gies are 432 kJ/mol and 318 kJ/mol, respectively [60]. Other than explaining the negative Δ for smaller w , the difference might be at the origin of a competition between the passivation of the nanowire and the formation of a H_2 phase. We can expect that this competition becomes increasingly important as the temperature T increases, possibly explaining the noticeable expansion of the surface area for H-SiNW. Interestingly, we note that despite the strong negative value of Δ for O-SiNW, which should promote the surface formation, the cross-section of the SiNW is actually shrinking, see the Supplementary Fig. S3 [53].

B. Thermal conductivity coefficient

In Fig. 4 we show the variation of κ with w . For comparison, we have also included earlier published simulation [20, 22, 23, 25, 61, 62] and experimental data [8, 15, 18, 19, 63]. Consistent with the experiments, our data also show the expected trend, i.e., κ decreases monotonically with decreasing w . This is not surprising given that lateral miniaturization leads to an enhanced phonon scattering by the surfaces. It can also be seen that our simulation and some experimental data sets [18, 19, 63] show the same linear variation, i.e., $1/\kappa = 1/\kappa_{\infty} + \alpha/w$ with the same prefactor α . This, however, we believe to be a mere coincidence because: (a) L in experiments are significantly larger than in our simulations and κ is known to increase with increasing L [40, 45], especially for the quasi-one-dimensional materials. (b) A quantitative comparison between the computationally com-

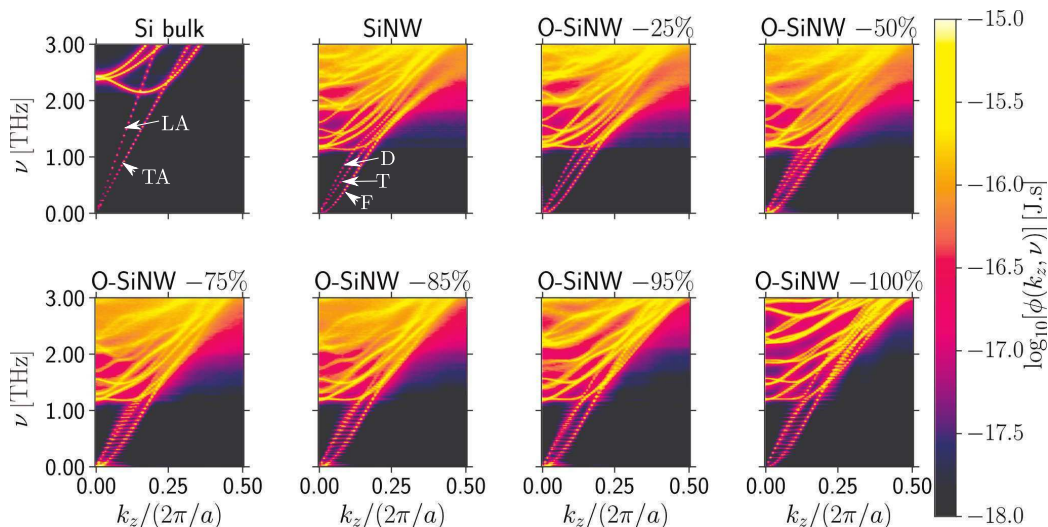


FIG. 6: Spectral energy density (SED) of the oxygen passivated silicon nanowires (O-SiNW) for different surface coverage concentrations c . For the reference, we have also included SED of bulk silicon and for a bare SiNW. Note that SED is calculated only including the silicon atoms. Data is shown for the smallest cross-section $w = 4a$. For the clarity of presentation, we have annotated the longitudinal (L) and transverse (T) acoustic branches for a bulk Si and the dilatational (D), the torsional (T), and the flexural (F) branches are highlighted for SiNW. Note that the D, T, and F branches can also be seen for the O-SiNWs. Moreover, the D and T branches merge for $c \geq 75\%$.

puted and experimentally observed κ values is not possible within the classical simulations. The scenario (b) is due to the fact that in a classical simulation all modes contribute equally to c_v , while in reality many modes are quantum mechanically frozen below Θ_D and thus do not contribute to c_v [64, 65]. This leads to an overestimation of c_v and thus also κ in classical simulation in comparison to the experiments [66]. Additionally, the phonon life time calculated within the classical simulations may also change due to the difference in the phonon distribution. It can also be seen that a few earlier simulations have shown opposite trends, i.e., κ increases for w below $\approx 2 - 3$ nm [23, 25, 61]. This non-monotonous change with decreasing w was discussed in relation to the phonon-boundary scattering to hydrodynamic phonon flow, which for the Tersoff potential, this transition has been located below 2 nm [25]. In this context, recent studies have shown that the hydrodynamic effects may play an important role [67, 68]. However, in our case, due to extreme confinement, these effects are negligible. Note that the data sets presented in Fig. 4 are obtained at different T , L and also by different methods. However, given that all the data were obtained for $T < \Theta_D$, the generic trend, i.e., $\kappa \propto w$, should remain the same, irrespectively of the system parameters and thus provides a robust overall picture of κ in SiNWs.

Fig. 4 presents the importance of lateral miniaturization as a common protocol to tune κ [8, 15, 18, 19, 22, 62, 63], while our results show that passivation provides an additional tuning parameter for κ . In Fig. 5 it can be appreciated that κ first decreases with increasing c (for $c \leq 50\%$ for O-SiNW and $c \leq 75\%$ for H-SiNW), then again increases when $c \rightarrow 100\%$. It is also evident that

O-SiNW shows a greater variation in κ than H-SiNW. What causes such non-monotonous variation in κ with c ? To answer this question, we focus on the phonon spectrum and compute the spectral energy density (SED) using [47–49].

C. Spectral energy density

In Fig. 6 we show SED data for O-SiNW systems for different c . For reference, we have also calculated SED for bulk Si and bare SiNW. Fig. 6 shows several interesting features:

1. SiNWs have rather complex phonon band structures compared to a bulk Si. For $\nu < 1.0$ THz, SiNWs show the dilatational (D), the torsional (T), and the flexural (F) acoustic branches in the decreasing order of (slope) group velocity, respectively (see the labeling for SiNW). More importantly, the emergence of slow flexural phonons in the long wavelength acoustic limit can be seen, i.e., following $\nu \propto k_z^2$.
2. The partial confinement of the optical phonons can also be observed, identified by the flat dispersion of the optical branches near $\nu \approx 1.2$ THz. Consistent with the literature, the D and T phonon branches (following $\nu \propto k_z$) become softer for SiNW than the bulk Si and thus also reduces κ [69].
3. The O-SiNW SED maps become sharper with increasing c , especially for $c \geq 75\%$. This is a clear indication of the improved crystallinity in O-SiNWs.

The spectral width of the branches is also inversely proportional to the phonon lifetime τ_p [47], i.e., the sharper the SED map, the higher the τ_p and thus an increase κ .

4. Fig. 6 also reveal that the acoustic phonon branches steepen up with increasing c and has a profound influence on the (intermediate) T branch., i.e., the T branch approaches the D branch with increasing c . Furthermore, there is a corresponding increase in the number of active phonon branches which changes the vibrational density of states $g(\nu)$ (see the Supplementary Figure S2) [53].
5. Passivation can also significantly change the flexural stiffness and hence group velocities (see the Supplementary Movie). The presence of the flexural stiffness significantly influence the phonon propagation. Larger flexural stiffness induces less number of kinks/bends along the O–SiNWs and thus have less number of phonon scattering sites for a given L_z [70–73].

To summarize the above observations– when only a small amount of passivated atoms are deposited onto the surfaces (i.e., $c \leq 65\%$), they arrange randomly and improves crystallinity only in the local surface patches. This, however, does not introduce any long range order (as evident from rather diffused bands in Fig. 6 for $c \leq 65\%$). On the contrary, within this c –regime, the passivated atoms act as the surface defects for phonon scattering and thus results in the initial decrease in κ with c in Fig. 5.

Further increase of κ for $c > 65\%$ is because of two collective effects: (a) the improved overall crystallinity (as evident from Fig. 6) and (b) stiffening of SiNWs via passivation, as indicated by the shift in the phonon peaks in $g(\nu)$ (see the Supplementary Fig. S2).

We note in passing that the observed non–monotonic trend in Fig. 5 is a generic effect that is not only observed for a set of passivated SiNW, but rather any quasi–one–dimensional system with the defect engineering via passivation shows the same trend. A typical example is the bottle–brush polymers, where the concentration of side molecules controls the flexural stiffness and heat leakage along the backbone [73].

We would also like to highlight that κ for H–SiNW is larger than for O–SiNW when $c < 80\%$ and show a shallower variation in κ with c . While we can not provide an exact quantitative reason for this issue, we would like to point out that the H–SiNWs have slightly larger cross–section than O–SiNW, see the Supplementary Fig. S3. This indicates that the surface stresses are likely to be larger for H–SiNW samples and thus is consistent with the larger κ values for $c < 80\%$. The increased κ for O–SiNW for $c > 80\%$ is because of the increased flexural stiffness of a O–SiNW in comparison to a H–SiNW.

We also comment that the surface passivation not only helps stabilize a SiNW, but it also improves the bulk

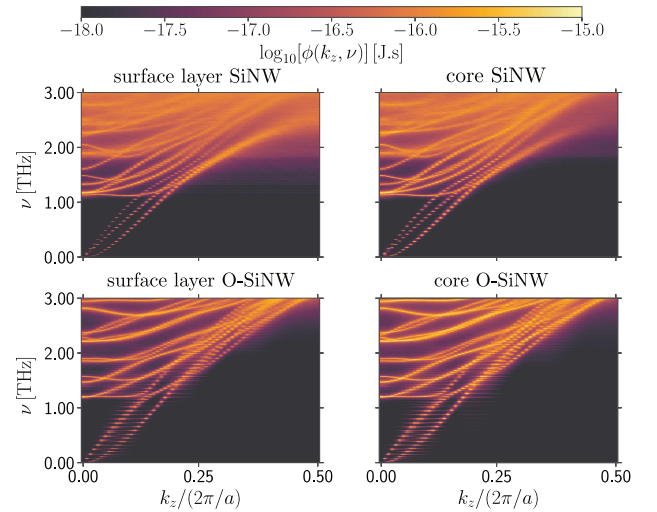


FIG. 7: Spectral energy density $\phi(k, \nu)$ of the surface (left panels) and core (right panels) Si atoms for SiNW and O–SiNW samples. The data is shown for a cross–section width of $w = 4a$. The data is shown for $c = 100\%$ surface passivation.

crystallinity. To validate this we have calculated the SED contributions from the bulk and surface Si atoms separately. In Fig. 7 we show SED for a SiNW and a O–SiNW for $w = 4a$. It can be appreciated that the amorphous surface Si atoms also affect the bulk crystallinity (seen by the rather diffused SED branches in the top panels of Fig. 7), while O–passivation improves surface crystallinity and thus also that of the bulk (see the bottom panels in Fig. 7). Note that this behavior is most dominant for $w \leq 10a$. For the the larger w amorphous Si surface does not significantly affect the bulk crystallinity, see the simulation snapshot in Supplementary Fig. S1 [53].

Lastly, to study the relative contribution of the surface modes to thermal transport, we have also computed $\phi^{\text{surf}}/\phi^{\text{core}}$. For the bare SiNWs (see the left panel in Fig. 8), it can be seen that D and F branches are dominated by the Si atoms at the core ($\phi^{\text{surf}}/\phi^{\text{core}} < 1$), while the surfaces and the core contribute equally to the T branch ($\phi^{\text{surf}}/\phi^{\text{core}} \simeq 1$). Note also that the red region within the range $k_z/(2\pi/a) \in [0.25; 0.50]$ and $\nu > 1$ THz is likely due to some background noise by the surface atoms.

The case of O–SiNW is somewhat different. For example, it can be seen from the right panel in Fig. 8 that the surface and the core contribute almost equally (i.e., $\phi^{\text{surf}}/\phi^{\text{core}} \simeq 1$). This explains that not only the surface crystallization that contributes to increase κ , instead a delicate balance between the surface crystallinity and the stiffness of an O–SiNW contributes to κ . A comparative comparison of the flexural vibrations between O–SiNW and H–SiNW is shown in the Supplementary Movie. This can be explained based on the fact that the passivation induces surface stress which increases the elastic torsional stiffness.

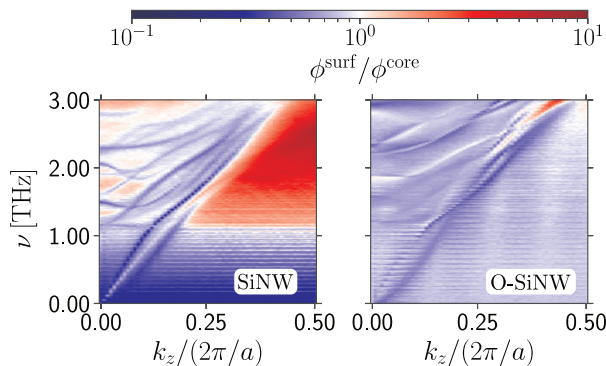


FIG. 8: The ratio of spectral energy density (SED) computed for the Si atoms on the outermost layer of the nanowires with respect to the Si atoms in the core. Data is shown for the bare silicon nanowires SiNW (left panel) and oxygen-passivated nanowires O-SiNW (right panel). The data is shown for $c = 100\%$ surface passivation.

IV. CONCLUSION

We have studied thermal transport κ in surface passivated silicon nanowires (SiNW) using classical molecular dynamics. Consistent with experimental data, our results indicate that SiNWs become rather unstable and amorphous for small cross-section widths, which can be attributed to a large excess energy Δ of the surface silicon atoms. We used Δ as a guiding tool to stabilize the SiNW surfaces via surface passivation. As an added advantage, the concentration of passivation provides an additional tuning parameter for thermal conductivity. When the surfaces remain crystalline due to the passivated atoms, they also increase the stiffness of a SiNW and thus show that a delicate balance between different system parameters controls the tunability in κ . Using the phonon band structure analysis, we also decouple the surface and the bulk effects on κ .

The discussion presented in this work thus highlights that the κ -behavior of SiNWs and passivated SiNWs is dictated by a delicate balance between different factors, i.e., surface-to-bulk crystallinity, flexural vibrations,

and stiffness via passivation. Therefore, it presents a microscopic picture of the heat flow in the surface treated low dimensional systems.

Supplementary Material: This document contains supporting data for some of the claims made in the main manuscript text. In particular, simulation snapshots for the large cross-section SiNWs, vibrational density of states for SiNW with passivation, and effect of passivation on SiNW cross-section are discussed.

Acknowledgement: C.R. gratefully acknowledges MITACS and Lumiense Photonics Inc. for the financial support. C.R. further thanks Daniel Bruns for useful discussions and Pierre Chapuis for the help with the representations of SiNWs. We thank the generous allocation of GPU hours to D.M. at the ARC Sockeye facility where majority of simulations are performed. Some simulations were also performed at the Compute Canada allocation to A.N. For D.M. and A.N. this research was undertaken thanks, in part, to the Canada First Research Excellence Fund (CFREF), Quantum Materials and Future Technologies Program.

Data availability: The scripts and the data associated with this research are available upon reasonable request from the corresponding author.

Author Contributions: C.R. wrote the LAMMPS scripts, ran the simulations, and analyzed the data. R.C.H. proposed the excess energy calculations and C.R. and R.C.H. co-analyzed the excess energy data. C.R., R.H., D.M., A.N., and S.P. proposed, designed, and conceptualized this study. C.R. and D.M. wrote the draft and all authors contributed to the editing. R.H., D.M., A.N., and S.P. contributed equally to this work and their names are written alphabetically. D.M. wrote the reply to the referees and the revised draft.

Competing interests: The authors declare no competing interests.

-
- [1] Sebastian G. Volz and Gang Chen. Molecular-dynamics simulation of thermal conductivity of silicon crystals. *Phys. Rev. B*, 61:2651–2656, Jan 2000.
- [2] M S Gudiksen, Lincoln J. Lauhon, Jianfang Wang, David C. Smith, and Charles M. Lieber. Growth of nanowire superlattice structures for nanoscale photonics and electronics. *Nature*, 415:617–620, 2002.
- [3] Yajie Dong, Guihua Yu, Michael C. McAlpine, Wei Lu, and Charles M. Lieber. Si/a-si core/shell nanowires as nonvolatile crossbar switches. *Nano Letters*, 8(2):386–391, 2008.
- [4] Sung Hyun Jo, Kuk-Hwan Kim, and Wei Lu. High-density crossbar arrays based on a si memristive system. *Nano Letters*, 9(2):870–874, 2009.
- [5] Thomas Mikolajick, André Heinzig, Jens Trommer, Sebastian Pregel, Matthias Grube, Gianauelio Cuniberti, and Walter M. Weber. Silicon nanowires – a versatile technology platform. *physica status solidi (RRL) – Rapid Research Letters*, 7(10):793–799, 2013.
- [6] Gang Zhang and Yong-Wei Zhang. Thermal conductivity of silicon nanowires: From fundamentals to phononic engineering. *physica status solidi (RRL) – Rapid Research Letters*, 7(10):754–766, 2013.
- [7] David G. Cahill, Paul V. Braun, Gang Chen, David R. Clarke, Shanhui Fan, Kenneth E. Goodson, Pawel Keblinski, William P. King, Gerald D. Mahan, Arun Ma-

- jumdar, Humphrey J. Maris, Simon R. Phillpot, Eric Pop, and Li Shi. Nanoscale thermal transport. ii. 2003–2012. *Applied Physics Reviews*, 1(1):011305, 2014.
- [8] Akram I Boukai, Yuri Bunimovich, Jamil Tahir-Kheli, Jen-Kan Yu, William A Goddard, III, and James R Heath. Silicon nanowires as efficient thermoelectric materials. *Nature*, 451(7175):168–171, January 2008.
- [9] Changwook Jeong, Supriyo Datta, and Mark Lundstrom. Thermal conductivity of bulk and thin-film silicon: A landauer approach. *Journal of Applied Physics*, 111(9):093708, 2012.
- [10] Shaimaa Elyamny, Elisabetta Dimaggio, Stefano Magagna, Dario Narducci, and Giovanni Pennelli. High power thermoelectric generator based on vertical silicon nanowires. *Nano Letters*, 20(7):4748–4753, 2020.
- [11] Renkun Chen, Jaeho Lee, Woonchul Lee, and Deyu Li. Thermoelectrics of nanowires. *Chemical Reviews*, 119(15):9260–9302, 2019.
- [12] Jin-Wu Jiang, Nuo Yang, Bing-Shen Wang, and Timon Rabczuk. Modulation of thermal conductivity in kinked silicon nanowires: Phonon interchanging and pinching effects. *Nano Letters*, 13(4):1670–1674, 2013.
- [13] Xavier Cartoixa, Riccardo Dettori, Claudio Melis, Luciano Colombo, and Riccardo Rurali. Thermal transport in porous si nanowires from approach-to-equilibrium molecular dynamics calculations. *Applied Physics Letters*, 109(1):013107, 2016.
- [14] Yang Zhao, Lin Yang, Chenhan Liu, Qian Zhang, Yunfei Chen, Juekuan Yang, and Deyu Li. Kink effects on thermal transport in silicon nanowires. *International Journal of Heat and Mass Transfer*, 137:573–578, 2019.
- [15] Allon I Hochbaum, Renkun Chen, Raul Diaz Delgado, Wenjie Liang, Erik C Garnett, Mark Najarian, Arun Majumdar, and Peidong Yang. Enhanced thermoelectric performance of rough silicon nanowires. *Nature*, 451(7175):163–167, January 2008.
- [16] Ling Liu and Xi Chen. Effect of surface roughness on thermal conductivity of silicon nanowires. *Journal of Applied Physics*, 107(3):033501, 2010.
- [17] Kathryn F. Murphy, Brian Piccione, Mehdi B. Zanjani, Jennifer R. Lukes, and Daniel S. Gianola. Strain- and defect-mediated thermal conductivity in silicon nanowires. *Nano Letters*, 14(7):3785–3792, 2014.
- [18] Deyu Li, Yiyang Wu, Philip Kim, Li Shi, Peidong Yang, and Arun Majumdar. Thermal conductivity of individual silicon nanowires. *Applied Physics Letters*, 83(14):2934–2936, 2003.
- [19] Jongwoo Lim, Kedar Hippalgaonkar, Sean C. Andrews, Arun Majumdar, and Peidong Yang. Quantifying surface roughness effects on phonon transport in silicon nanowires. *Nano Letters*, 12(5):2475–2482, 2012.
- [20] Sebastian G. Volz and Gang Chen. Molecular dynamics simulation of thermal conductivity of silicon nanowires. *Applied Physics Letters*, 75(14):2056–2058, 1999.
- [21] D. P. Sellan, J. E. Turney, A. J. H. McGaughey, and C. H. Amon. Cross-plane phonon transport in thin films. *Journal of Applied Physics*, 108(11):113524, 12 2010.
- [22] Zahid Rashid, Liyan Zhu, and Wu Li. Effect of confinement on anharmonic phonon scattering and thermal conductivity in pristine silicon nanowires. *Phys. Rev. B*, 97:075441, Feb 2018.
- [23] Inna Ponomareva, Deepak Srivastava, and Madhu Menon. Thermal conductivity in thin silicon nanowires: Phonon confinement effect. *Nano Letters*, 7(5):1155–1159, 2007.
- [24] Davide Donadio and Giulia Galli. Atomistic simulations of heat transport in silicon nanowires. *Phys. Rev. Lett.*, 102:195901, May 2009.
- [25] Yanguang Zhou, Xiaoliang Zhang, and Ming Hu. Non-monotonic diameter dependence of thermal conductivity of extremely thin si nanowires: Competition between hydrodynamic phonon flow and boundary scattering. *Nano Letters*, 17(2):1269–1276, 2017.
- [26] Yi Yu, Fan Cui, Jianwei Sun, and Peidong Yang. Atomic structure of ultrathin gold nanowires. *Nano Letters*, 16(5):3078–3084, 2016.
- [27] Maxime Verdier, David Lacroix, and Konstantinos Termentzidis. Roughness and amorphization impact on thermal conductivity of nanofilms and nanowires: Making atomistic modeling more realistic. *Journal of Applied Physics*, 126(16):164305, 10 2019.
- [28] A. J. Lu, R. Q. Zhang, and S. T. Lee. Tunable electronic band structures of hydrogen-terminated (112) silicon nanowires. *Applied Physics Letters*, 92(20):203109, 05 2008.
- [29] Robinson Cortes-Huerto, Jacek Goniakowski, and Claudine Noguera. An efficient many-body potential for the interaction of transition and noble metal nano-objects with an environment. *The Journal of Chemical Physics*, 138(24):244706, 2013.
- [30] Robinson Cortes-Huerto, Jacek Goniakowski, and Claudine Noguera. Role of the environment in the stability of anisotropic gold particles. *Phys. Chem. Chem. Phys.*, 17:6305–6313, 2015.
- [31] R. He, D. Gao, R. Fan, A.I. Hochbaum, C. Carraro, R. Maboudian, and P. Yang. Si nanowire bridges in microtrenches: Integration of growth into device fabrication. *Advanced Materials*, 17(17):2098–2102, 2005.
- [32] Yi Cui, Zhaohui Zhong, Deli Wang, Wayne U. Wang, and Charles M. Lieber. High performance silicon nanowire field effect transistors. *Nano Letters*, 3(2):149–152, 2003.
- [33] Hwa Young Kim, Jeunghee Park, and Hyunik Yang. Synthesis of silicon nitride nanowires directly from the silicon substrates. *Chemical Physics Letters*, 372(1):269–274, 2003.
- [34] E S M Ashour, M Y Sulaiman, N Amin, and Z Ibrahim. Silicon nitride passivation of silicon nanowires solar cell. *Journal of Physics: Conference Series*, 431(1):012021, apr 2013.
- [35] H. P. Li, Abir De Sarkar, and R. Q. Zhang. Surface-nitrogenation-induced thermal conductivity attenuation in silicon nanowires. *Europhysics Letters*, 96(5):56007, nov 2011.
- [36] J. Tersoff. New empirical approach for the structure and energy of covalent systems. *Phys. Rev. B*, 37:6991–7000, Apr 1988.
- [37] Shinji Munetoh, Teruaki Motooka, Koji Moriguchi, and Akira Shintani. Interatomic potential for si-o systems using tersoff parameterization. *Computational Materials Science*, 39(2):334–339, 2007.
- [38] F. de Brito Mota, J. F. Justo, and A. Fazzio. Hydrogen role on the properties of amorphous silicon nitride. *Journal of Applied Physics*, 86(4):1843–1847, 1999.
- [39] Aidan P. Thompson, H. Metin Aktulga, Richard Berger, Dan S. Bolintineanu, W. Michael Brown, Paul S. Crozier, Pieter J. in ’t Veld, Axel Kohlmeyer, Stan G. Moore, Trung Dac Nguyen, Ray Shan, Mark J. Stevens, Julien Tranchida, Christian Trott, and Steven J. Plimpton.

- Lammps - a flexible simulation tool for particle-based materials modeling at the atomic, meso, and continuum scales. *Computer Physics Communications*, 271:108171, 2022.
- [40] E. Lampin, P. L. Palla, P.-A. Francioso, and F. Cleri. Thermal conductivity from approach-to-equilibrium molecular dynamics. *Journal of Applied Physics*, 114(3):033525, 2013.
- [41] Daan Frenkel and Berend Smit. *Understanding molecular simulation*. Academic Press, UK, 2002.
- [42] Charles Kittel. *Introduction to Solid State Physics, Eighth Edition*. John Wiley & Sons, 2005.
- [43] Zheyong Fan, Yanzhou Wang, Xiaokun Gu, Ping Qian, Yanjing Su, and Tapio Ala-Nissila. A minimal Tersoff potential for diamond silicon with improved descriptions of elastic and phonon transport properties. *Journal of Physics: Condensed Matter*, 32(13):135901, dec 2019.
- [44] C. J. Glassbrenner and Glen A. Slack. Thermal conductivity of silicon and germanium from 3°K to the melting point. *Phys. Rev.*, 134:A1058–A1069, May 1964.
- [45] Daniel Bruns, Alireza Nojeh, A. Srikantha Phani, and Jörg Rottler. Heat transport in carbon nanotubes: Length dependence of phononic conductivity from the Boltzmann transport equation and molecular dynamics. *Phys. Rev. B*, 101:195408, May 2020.
- [46] Robert Zwanzig. Time-correlation functions and transport coefficients in statistical mechanics, 1965.
- [47] John A. Thomas, Joseph E. Turney, Ryan M. Iutzi, Cristina H. Amon, and Alan J. H. McGaughey. Predicting phonon dispersion relations and lifetimes from the spectral energy density. *Phys. Rev. B*, 81:081411, Feb 2010.
- [48] John A. Thomas, Joseph E. Turney, Ryan M. Iutzi, Cristina H. Amon, and Alan J. H. McGaughey. Erratum: Predicting phonon dispersion relations and lifetimes from the spectral energy density [Phys. Rev. B 81, 081411(r) (2010)]. *Phys. Rev. B*, 91:239905, Jun 2015.
- [49] Hossein Honarvar and Mahmoud I. Hussein. Spectral energy analysis of locally resonant nanophononic metamaterials by molecular simulations. *Phys. Rev. B*, 93:081412, Feb 2016.
- [50] Tianli Feng, Bo Qiu, and Xiulin Ruan. Anharmonicity and necessity of phonon eigenvectors in the phonon normal mode analysis. *Journal of Applied Physics*, 117(19):195102, 2015.
- [51] Charles L. Cleveland and Uzi Landman. The energetics and structure of nickel clusters: Size dependence. *The Journal of Chemical Physics*, 94(11):7376–7396, 1991.
- [52] F. Baletto, R. Ferrando, A. Fortunelli, F. Montalenti, and C. Mottet. Crossover among structural motifs in transition and noble-metal clusters. *The Journal of Chemical Physics*, 116(9):3856–3863, 03 2002.
- [53] Electronic supplementary material. document number to be included by the editor.
- [54] Hai peng Li and Rui qin Zhang. Anomalous effect of hydrogenation on phonon thermal conductivity in thin silicon nanowires. *Europhysics Letters*, 105(5):56003, mar 2014.
- [55] H. Hofmeister, F. Huisken, and B. Kohn. Lattice contraction in nanosized silicon particles produced by laser pyrolysis of silane. *The European Physical Journal D - Atomic, Molecular, Optical and Plasma Physics*, 9(1):137–140, 1999.
- [56] D. K. Yu, R. Q. Zhang, and S. T. Lee. Structural transition in nanosized silicon clusters. *Phys. Rev. B*, 65:245417, Jun 2002.
- [57] Jason L. Pitters, Lucian Livadaru, M. Baseer Haider, and Robert A. Wolkow. Tunnel coupled dangling bond structures on hydrogen terminated silicon surfaces. *The Journal of Chemical Physics*, 134(6):064712, 2011.
- [58] M.I. Bertoni, S. Hudelson, B.K. Newman, D.P. Fenning, H.F.W. Dekkers, E. Cornagliotti, A. Zuschlag, G. Micard, G. Hahn, G. Coletti, B. Lai, and T. Buonassisi. Influence of defect type on hydrogen passivation efficacy in multicrystalline silicon solar cells. *Progress in Photovoltaics: Research and Applications*, 19(2):187–191, 2011.
- [59] Roshan Achal, Mohammad Rashidi, Jeremiah Croshaw, Taleana R. Huff, and Robert A. Wolkow. Detecting and directing single molecule binding events on h-si(100) with application to ultradense data storage. *ACS Nano*, 14(3):2947–2955, 2020.
- [60] J. E. Huheey, E. A. Keiter, and R. L. Keiter. *Inorganic Chemistry—Principles of Structure and Reactivity*. HarperCollins College, 4 edition, 1993.
- [61] Davide Donadio and Giulia Galli. Temperature dependence of the thermal conductivity of thin silicon nanowires. *Nano Letters*, 10(3):847–851, 2010.
- [62] David Lacroix, Karl Joulain, Damian Terris, and Denis Lemonnier. Monte Carlo simulation of phonon confinement in silicon nanostructures: Application to the determination of the thermal conductivity of silicon nanowires. *Applied Physics Letters*, 89(10):103104, 2006.
- [63] Jaeho Lee, Wochul Lee, Jongwoo Lim, Yi Yu, Qiao Kong, Jeffrey J. Urban, and Peidong Yang. Thermal transport in silicon nanowires at high temperature up to 700 K. *Nano Letters*, 16(7):4133–4140, 2016.
- [64] Jürgen Horbach, Walter Kob, and Kurt Binder. Specific heat of amorphous silica within the harmonic approximation. *The Journal of Physical Chemistry B*, 103(20):4104–4108, 1999.
- [65] Hongyu Gao, Tobias P. W. Menzel, Martin H. Müser, and Debashish Mukherji. Comparing simulated specific heat of liquid polymers and oligomers to experiments. *Phys. Rev. Mater.*, 5:065605, Jun 2021.
- [66] M. Lim, Z. Rak, J. L. Braun, C. M. Rost, G. N. Kotsonis, P. E. Hopkins, J.-P. Maria, and D. W. Brenner. Influence of mass and charge disorder on the phonon thermal conductivity of entropy stabilized oxides determined by molecular dynamics simulations. *Journal of Applied Physics*, 125:055105, 2019.
- [67] Xin Huang, Yangyu Guo, Yunhui Wu, Satoru Masubuchi, Kenji Watanabe, Takashi Taniguchi, Zhongwei Zhang, Sebastian Volz, Tomoki Machida, and Masahiro Nomura. Observation of phonon poiseuille flow in isotopically purified graphite ribbons. *Nature Communications*, 14(1):2044, Apr 2023.
- [68] Paul Desmarchelier, Albert Beardo, F. Xavier Alvarez, Anne Tanguy, and Konstantinos Termentzidis. Atomistic evidence of hydrodynamic heat transfer in nanowires. *International Journal of Heat and Mass Transfer*, 194:123003, 2022.
- [69] David G. Cahill, S. K. Watson, and R. O. Pohl. Lower limit to the thermal conductivity of disordered crystals. *Phys. Rev. B*, 46:6131–6140, Sep 1992.
- [70] Jin-Wu Jiang, Nuo Yang, Bing-Shen Wang, and Timon Rabczuk. Modulation of thermal conductivity in kinked silicon nanowires: Phonon interchanging and pinching effects. *Nano Letters*, 13(4):1670–1674, 2013.

- [71] Xuhui Duan, Zehuan Li, Jun Liu, Gang Chen, and Xiaobo Li. Roles of kink on the thermal transport in single polyethylene chains. *Journal of Applied Physics*, 125(16), 04 2019. 164303.
- [72] Aashish Bhardwaj, A. Srikantha Phani, Alireza Nojeh, and Debashish Mukherji. Thermal transport in molecular forests. *ACS Nano*, 15(1):1826–1832, 2021.
- [73] Manoj Kumar Maurya, Tobias Laschuetza, Manjesh Kumar Singh, and Debashish Mukherji. Thermal conductivity of bottle-brush polymers. *Langmuir*, 40(8):4392–4400, 2024. PMID: 38363586.

This figure "kappa_vs_cross-section.png" is available in "png" format from:

<http://arxiv.org/ps/2304.11707v3>